



1 **Validation of modeled snow properties in Afghanistan, Pakistan, and Tajikistan**

2

3 Edward H. Bair¹, Karl Rittger², Jawairia A. Ahmad³, and Doug Chabot⁴

4

5 ¹Earth Research Institute, University of California, Santa Barbara, California, USA

6 6832 Ellison Hall, University of California, Santa Barbara, CA 93106-3060. correspondence

7 email: nbair@eri.ucsb.edu

8

9 ²Institute for Arctic and Alpine Research, University of Colorado, Boulder, Colorado, USA

10

11 ³Department of Civil & Environmental Engineering, University of Maryland, College Park, MD,

12 USA

13

14 ⁴independent researcher, Bozeman, MT, USA



15 ABSTRACT: Ice and snowmelt feed the Indus and Amu Darya rivers, yet there are limited in situ
16 measurements of these resources. Previous work in the region has shown promise using snow
17 water equivalent (SWE) reconstruction, which requires no in situ measurements, but validation
18 has been a problem until recently when we were provided with daily manual snow depth
19 measurements from Afghanistan, Tajikistan, and Pakistan by the Aga Khan Agency for Habitat
20 (AKAH). For each station, accumulated precipitation and SWE were derived from snow depth
21 using the SNOWPACK model. High-resolution (500 m) reconstructed SWE estimates from the
22 ParBal model were then compared to the modeled SWE at the stations. The Alpine3D model was
23 then used to create spatial estimates at 25 km to compare with estimates from other snow
24 models. Additionally, the coupled SNOWPACK and Alpine3D system has the advantage of
25 simulating snow profiles, which provide stability information. Following previous work, the
26 median number of critical layers and percentage of facets across all of the pixels containing the
27 AKAH stations was computed. For SWE at the point scale, the reconstructed estimates showed a
28 bias of -42 mm (-19%) at the peak. For the coarser spatial SWE estimates, the various models
29 showed a wide range, with reconstruction being on the lower end. For stratigraphy, a heavily
30 faceted snowpack is observed in both years, but 2018, a dry year, according to most of the
31 models, showed more critical layers that persisted for a longer period.



32 1 INTRODUCTION

33 There are many parts of the world where little is known about the snowpack. This lack of
34 knowledge presents a challenge for water managers and for avalanche forecasters. Afghanistan is
35 particularly austere in this respect, as there have been no snow measurements available since the
36 early 1980s. This lack of information about the snowpack potentially creates a humanitarian
37 crisis, as snowmelt fed streams run dry in the fall without warning (USAID, 2008). Accurate
38 historical estimates of basin-wide snow water equivalent (SWE) are crucial for creating a
39 baseline of climatological conditions, which can then aid in predicting today's SWE. For
40 example, climatological estimates of spatially-distributed SWE are the most important predictors
41 in machine learning statistical models for this region (Bair et al., 2018b).

42 To improve our knowledge about the snowpack in these areas, we have developed an approach
43 that requires no in situ measurements. Using satellite-based estimates of the fractional snow-
44 covered area (fSCA) and downscaled forcings in an energy balance model, we build up the
45 snowpack in reverse, from melt out to its peak, using a technique called SWE reconstruction
46 (Martinec and Rango, 1981). This technique has been shown to accurately estimate SWE in
47 mountain ranges across the world, including: the Sierra Nevada USA (Bair et al., 2016; Rittger et
48 al., 2016); the Rocky Mountains USA (Jepsen et al., 2012; Molotch, 2009); and the Andes of
49 South America (Cornwell et al., 2016)—all areas with relatively abundant independent ground
50 validation measurements. For the so called Third Pole of High Mountain Asia, and especially the
51 northwestern parts of this region, e.g. Afghanistan, Tajikistan, and Pakistan, ground-based
52 validation is challenging.

53 2 AGA KHAN AGENCY FOR HABITAT (AKAH) STATIONS

54 In 2017, we received daily manual snow depth and other meteorological measurements from
55 nearly 100 stations (Figure 1) in an operational avalanche network (Chabot and Kaba, 2016).
56 These stations are funded by the Aga Khan Agency for Habitat (AKAH) and are the first
57 snowpack measurements available, at least that we are aware of, in Afghanistan in nearly 40
58 years. Hence, we refer to the region as the AKAH study region and the weather stations as the
59 AKAH stations. The AKAH stations contain manual daily snow depth (also called height of
60 snow), height of new (24-hr) snow, daily high and low air temperature, instantaneous wind
61 speed/direction, rainfall, and some text fields on weather and avalanche conditions. For
62 mountainous areas, precipitation is the most uncertain term in the water balance (Adam et al.,
63 2006; Milly and Dunne, 2002) because it exhibits high spatial variability and is difficult to
64 measure with traditional gauges. Measuring snow on the ground has many advantages compared
65 to using precipitation gauges, which suffer from undercatch, especially in the windy and treeless
66 areas (Goodison et al., 1998; Kochendorfer et al., 2017; Lehning et al., 2002a) typical of this part
67 of the world. Likewise, a strength of the SWE reconstruction technique is that it does not depend
68 on precipitation measurements to build the snowpack.

69 Additionally, many of the AKAH stations are at high altitudes, with 64 stations above 2500 m
70 and 17 stations above 3000 m. Unfortunately, most of these stations are located in deep valleys,
71 where the villages are, rather than on exposed mountain sides or ridges and the daily resolution is
72 too coarse to use in a snow model without temporal interpolation. Additionally, many of the
73 stations are near glacierized areas which complicates spatially interpolated snow estimates, as
74 some of the snow is on top of ice. The area covered by glaciers in Figure 1 is 7.8%.

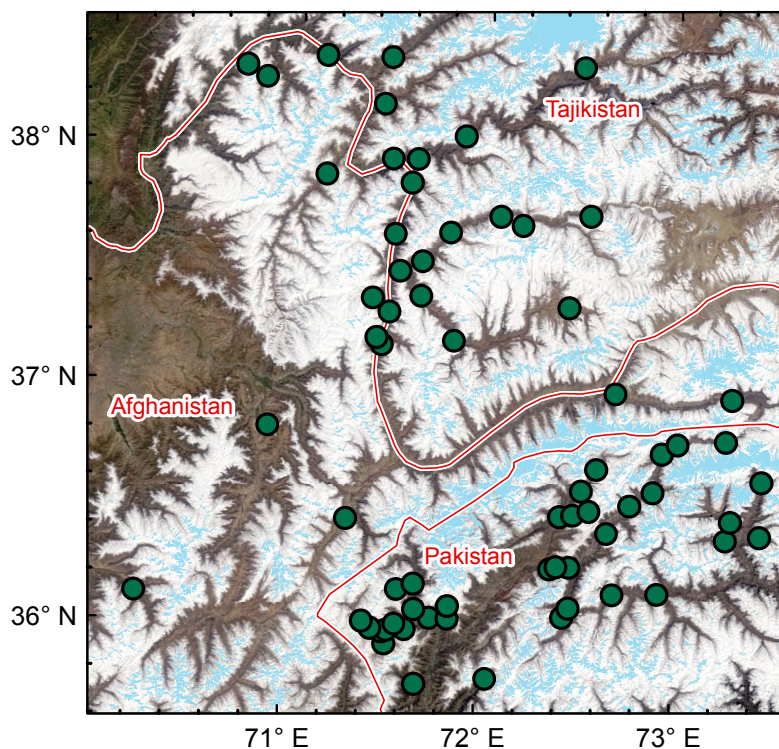


Figure 1 Study region with AKAH stations (green dots) overlaid on a MODIS true color image from 13 April 2018. Also shown are the country boundaries (red) and glacierized areas (light blue) from the Global Land Ice Measurement from Space dataset (Raup et al., 2007). All of the stations in Afghanistan and Tajikistan eventually flow into the Amu Darya River. All of the stations in Pakistan eventually flow into the Indus River.

75

76 Although there have been a large number of studies examining the glaciers of High Mountain
77 Asia, there are fewer studies examining snowfall in High Mountain Asia, which is odd since
78 hydrologically in this region, snow on land melt provides the vast majority of runoff compared to
79 snow on ice and melting glacier ice (Armstrong et al., 2018). Many of these studies are focused
80 on the region to the east of the AKAH study area shown in Figure 1. To our knowledge, there
81 have been no studies on snowpack stratigraphy in the AKAH study area and we were unable to
82 obtain any snow pit measurements from this area.

83 3 LITERATURE REVIEW

84 A few studies have specifically examined snowfall in larger regions that include some of the
85 AKAH stations, mostly for stations in the southern basins that flow into the Indus River; that is
86 all of the stations in Pakistan. The rest of the stations in Afghanistan and Tajikistan flow into the
87 Amu Darya River. The most comparable study (Shakoor and Ejaz, 2019) examines the Passu
88 catchment in the Hunza River Basin, to the east of Figure 1. As in this study (Section 5.1),
89 Shakoor and Ejaz (2019) also use the SNOWPACK and Alpine3D models. Model parameters
90 were calibrated using a single weather station, Urdukas at 3926 m elevation near the Baltoro



91 glacier (Ev-K2-CNR, 2014), with one year of precipitation measurements, using snow depth for
92 validation. The authors report overestimation of the measured snow depth at the calibration
93 station, even after questionable adjustments to the snow albedo and other model parameters.
94 They attribute the overestimation to problems with the precipitation measurements, common for
95 high altitude stations. One problem with the Urdukas station in particular is that the tipping
96 bucket precipitation gauge is unheated, making it unusable for measuring solid precipitation.
97 Temperatures at this station were well below freezing for the winter and most of the spring,
98 which explains why no precipitation was recorded from January until sometime in March during
99 2012, the calibration year.

100 Viste and Sorteberg (2015) study several gridded precipitation products throughout High
101 Mountain Asia, including the Indus River Basin. They report that while total precipitation was
102 similar across the products—including MERRA (Rienecker et al., 2011), APHRODITE, TRMM
103 (Huffman et al., 2007), and CRU (Harris et al., 2014)—the total snowfall varied by 2 to 4 ×.
104 Smith and Bookhagen (2018) used 24 years (1987 to 2009) of satellite-based passive microwave
105 SWE estimates to examine trends throughout High Mountain Asia, including the Amu Darya and
106 Indus Basins. Their SWE estimates show most 25 km pixels in this region in the 50-100 mm
107 range for December through February, with a few over 100 mm in the Amu Darya (i.e. all the
108 AKAH stations in Afghanistan and Tajikistan) and none over 100 mm in the Indus (i.e. all the
109 AKAH stations in Pakistan), likely too low by an order of magnitude for some pixels given our
110 previous reconstructed SWE values and limited climate measurements in Afghanistan (Bair et
111 al., 2018b).

112 For the AKAH stations in Tajikistan, the most comprehensive snow measurements come from
113 Soviet snow surveys (mostly depth, but with some SWE and density measurements) that have
114 been digitized (Bedford and Tsarev, 2001). Most of these measurements begin in the late 1950s
115 and end around the fall of the Soviet Union, in either 1990 or 1992, making them useful for
116 climatological studies, but not for validation of modern satellite-based estimates.

117 The sole source of snow measurements in Afghanistan that were accessible to us was a table of
118 outdated WMO monthly climatological data from Kabul (el. 1791 m) and North Salang (el. 3366
119 m), showing the maximum monthly snow depth and the mean number of days with snow (Table
120 1 in Bair et al., 2018b). Again, these measurements are not useful to validate more modern snow
121 estimates.

122 There have been many other studies that have attempted to estimate basin-wide precipitation
123 (including snowfall) for larger areas that include the AKAH region, especially in the Indus.
124 Several climate studies of the Indus have focused on using lower elevation precipitation gauges,
125 which are then used to spatially interpolate basin-wide precipitation. Dahri et al. (2016) and
126 Dahri et al. (2018) have assembled perhaps the largest collection of climatological measurements
127 covering the AKAH region, mostly based on gauge measurements, as part of a study on the
128 hydrometeorology of the Indus Basin. Using undercatch corrections based on wind, often from
129 reanalysis, they increased precipitation estimates by 21% on average throughout the Indus Basin
130 (Dahri et al., 2018). For example, in the Gilgit sub-basin, they find an unadjusted precipitation
131 estimate of 582 mm/year, adjusted to 787 mm/year, a 35% increase. Although some of the
132 measurements are taken from publicly available sources, as with most publications for this
133 region, the comprehensive data used are not publicly accessible.



134 A similar but less sophisticated approach was used by Lutz et al. (2014), who used a constant
135 increase of 17% across the APHRODITE (Yatagai et al., 2012) precipitation dataset which
136 covers all of High Mountain Asia. Immerzeel et al. (2015) used glacier mass balance estimates
137 with streamflow measurements as validation to show that high-altitude precipitation in the upper
138 Indus Basin is 2 to 10 × what is shown using gridded precipitation products like APHRODITE.
139 Bookhagen and Burbank (2010) estimate that snowmelt contributes 66% of annual discharge to
140 the Indus, and averages 424 mm across the basin.

141 In summary, quite a few studies have produced varying precipitation and snowfall estimates for
142 the AKAH region, with no recent in situ snow measurements from Afghanistan or Tajikistan.

143 4 PREVIOUS WORK WITH AKAH SNOW MEASUREMENTS

144 Our previous work (Bair et al., 2018b) used a simple density model (Sturm et al., 2010) based on
145 snow climatology (Sturm et al., 1995) and day of year to model SWE from the manual snow
146 depth measurements. The density model itself has -12 to 26% bias in predicting SWE. When
147 taking into account geolocational uncertainty of the reconstructed SWE estimates and
148 uncertainty in the density model, errors are on the order of 11-13% Mean Absolute Error (MAE)
149 and -2 to 4% bias, depending on the date. However, we only examined one year of the AKAH
150 station data (2017) and the high uncertainty in the density model itself begs a more sophisticated
151 approach.

152 From recent work (Bair et al., 2018a), we have shown that the SNOWPACK (Bartelt and
153 Lehning, 2002; Lehning et al., 2002a; Lehning et al., 2002b) model is capable of accurate SWE
154 prediction when supplied only with snow depth for precipitation, as well as the other requisite
155 forcings (i.e. radiation, snow albedo, temperatures, and wind speed). Over a 5-year period using
156 hourly in situ measured energy balance forcings and a snow pillow for validation at a high
157 elevation site in the western US, the SNOWPACK modeled SWE showed a bias of -17 mm or
158 1% (Bair et al., 2018a).

159 5 METHODS

160 Our modeling approach consisted of: a) downscaling forcings in ParBal and reconstructing SWE;
161 b) combining the downscaled forcings for each AKAH station with temporally interpolated
162 manual snow measurements; c) running SNOWPACK for each of the AKAH stations with the
163 downscaled and interpolated measurements from a) and b); and d) running Alpine3D using the
164 output from SNOWPACK, notably the hourly precipitation. In addition to predicting SWE, the
165 SNOWPACK/Alpine3D coupled model also predicts stratigraphic parameters useful for
166 avalanche prediction, thereby giving us an idea of the layering and stability in this region. For
167 comparison, we also ran the NOAH-MP land surface model over the region with widely-used
168 forcings. We also compared spatial estimates of SWE from GLDAS-2. Methods are summarized
169 in Table 1 and explained below, with more detail provided in Appendix A.

170 5.1 SNOWPACK and Alpine3D

171 SNOWPACK and Alpine3D are freely available (<https://models.slf.ch>) point and spatially
172 distributed snow models, courtesy of the Swiss Federal Snow Institute. SNOWPACK is the older
173 of the two and uses finite elements to model all of the layers in a snowpack at a point.



Model	Point comparison?	Spatial comparison?	Version	Forcings	Output
ParBal	√	√	1.0	CERES 4a (radiation); GLDAS-2 (meteorological); MODSCAG/MODDRFS (snow surface properties)	Daily reconstructed SWE at 500 m; hourly downscaled forcings at 500 m, both for entire AKAH study area
SNOWPACK	√		3.5	AKAH station snow measurements; downscaled forcings from ParBal	Hourly SWE, precipitation, and other forcings for each AKAH station
Alpine3D		√	3.1	AKAH station output from SNOWPACK	Daily SWE at 25 km for entire AKAH study area
NOAH MP		√	3.6	MERRA-2	Daily SWE at 25 km for entire AKAH study area
GLDAS		√	NOAH 2.1	various	Daily SWE at 25 km for entire AKAH study area

174 *Table 1 Summary of models used. See Section 5 and Appendix A for an explanation of acronyms and*
 175 *further details.*

176 SNOWPACK has shown promising results in both operational (e.g. Lehning et al., 1999;
 177 Nishimura et al., 2005) and research applications (e.g. Bellaire et al., 2011; Hirashima et al.,
 178 2010). Alpine3D (Lehning et al., 2006) is essentially a spatially-distributed version of
 179 SNOWPACK with a number of additional modules including: terrain-based radiation modeling,
 180 blowing snow, and hydrologic modeling. Integral to Alpine3D is SNOWPACK, which is run for
 181 each pixel, as well as the MeteoIO library (Bavay and Egger, 2014), which provides a large
 182 number of temporal and spatial interpolation functions that can be used on forcings for Alpine3D
 183 and SNOWPACK.

184 5.2 The Parallel Energy Balance Model

185 The Parallel Energy Balance Model (ParBal) was created at UC-Santa Barbara and designed for
 186 reconstruction of SWE. It is also publicly available
 187 (<https://github.com/edwardbair/ParBal/releases/tag/v1.0>). Currently, ParBal is designed to use:
 188 downscaled temperature, pressure, and humidity from version 2 of the Global or National Land
 189 Data Assimilation System (GLDAS-2/NLDAS-2, Rodell et al., 2004; Xia et al., 2012);
 190 shortwave and longwave radiation from edition 4a of the Clouds and the Earth's Radiant Energy
 191 System (CERES, Rutan et al., 2015) SYN product; and time-spaced smoothed (Dozier et al.,
 192 2008; Rittger et al., in press) snow surface properties from MODIS Snow Covered Area and
 193 Grain Size (MODSCAG, Painter et al., 2009) and MODIS Dust and Radiative Forcing in Snow



194 (MODRRFS, Painter et al., 2012). ParBal is run hourly at 500 m spatial resolution and forcings
195 are adjusted for terrain and elevation. The main output is the residual energy balance term, which
196 is assumed to go into melt when positive during the ablation phase after cold content is overcome
197 (Jepsen et al., 2012). This residual melt term is then summed in reverse during periods of
198 contiguous snow cover and multiplied by the fSCA to spread the snow spatially. Details on
199 ParBal are covered extensively in Bair et al. (2016) and Rittger et al. (2016).

200 5.3 NOAH Multi-Parameterization (MP)

201 The NOAH-MP v3.6 (Ek et al., 2003; Niu et al., 2011) land surface model, forced using
202 MERRA-2 (Gelaro et al., 2017), was used to simulate the hydrologic cycle over the study area
203 and provide SWE estimates for comparison with ParBal and the Alpine3D output. NOAH-MP
204 was selected due to its detailed representation of the snowpack relative to other land surface
205 models. The model subdivides the snowpack into up to three layers with associated liquid water
206 storage and melt/refreeze capability (Niu and Yang, 2004; Yang and Niu, 2003). It incorporates
207 the exchange of heat and moisture through the snowpack between the land surface and the
208 atmosphere. In a model intercomparison study using a 2 km spatial resolution regional climate
209 model for forcings, Chen et al. (2014) show that NOAH-MP modeled peak SWE at SNOTEL
210 sites in Colorado, USA with a -7% bias.

211 5.4 Use of AKAH station measurements

212 We modeled daily SWE at the AKAH stations during the 2017 and 2018 water years primarily
213 using the manually measured height of snow (HS), also called snow depth, combined with our
214 downscaled energy balance parameters (for downscaling methodology see Bair et al., 2018b;
215 Bair et al., 2016; Rittger et al., 2016). We choose the manual HS and new (24-hr) snow (HN) as
216 the only variables to use from the AKAH stations. The HS appeared to be the most reliably
217 measured, as that only requires reading a value from a master snow depth stake. The HN was
218 used to correct a data entry problem in 2017 that we discuss below. The reliability of the other
219 measurements (instantaneous wind speed/direction, maximum/minimum temperature, and
220 rainfall) was questionable. For example, we were not provided with sensor or measurement
221 metadata, e.g. sensor make/model, measurement height, and whether or not the temperature
222 sensor was shielded from shortwave radiation. These other measurements taken daily were also
223 of limited value for interpolation to hourly values (see item 3 below). Thus, these other
224 measurements were not used.

225 The AKAH dataset had a number of shortcomings that we list here along with how we addressed
226 them.

- 227 1) Some of the stations recorded no snow at all, especially in the dry 2018 year, or had obvious
228 problems, so they were excluded. For 2017, 52 (54%) of stations were used. For 2018, 41
229 (46%) stations were used.
- 230 2) There were spurious drops in the HS measurements. The drops were clearly cases of missing
231 values being filled with zeros. These measurements were manually flagged and converted to
232 null values for interpolation, see below.
- 233 3) The daily measurements had to be interpolated to hourly values. For the most part we used
234 linear interpolation, although this is not ideal during snow accumulation since it's almost



235 never the case that snowfall is uniform over a 24-hr period. This is a problem that affects the
236 accuracy of snow settlement estimated by SNOWPACK. There were two cases where other
237 interpolation methods were used. If there were several days of missing values, we used a
238 nearest neighbor interpolation to fill in the missing daily values, followed by a linear
239 interpolation from daily to hourly measurements such that we assumed all the new snow fell
240 in a 24-hr period. The other case was for days where the linear interpolation would yield a
241 value below the minimum threshold hard coded into SNOWPACK (0.5cm/hr) for the first
242 accumulating snowfall on bare ground. In this case, a previous neighbor interpolation was
243 used in such a way that the entire snowfall occurred in the last hr prior to the next day's
244 measurement.

245 4) We found the AKAH stations suitable for snow on the ground measurements, but not for
246 rainfall or total (solid+liquid) precipitation. This was only an issue for the Alpine3D snow
247 modeling, as snow measurements were being extrapolated to higher elevations than the
248 AKAH stations (Section 6.2), thus at these higher elevations, snow accumulated earlier and
249 melted later than at the lower AKAH stations.

250 Given the near total lack of canopy cover in the region, we suspected substantial undercatch from
251 rain gauges. Using the wind speed, an undercatch correction would have been possible given
252 more information on the gauges (e.g. orifice opening diameter and whether or not a shield was
253 present), however this instrument metadata was not available to us. Likewise, we did not know if
254 the gauges were heated or not.

255 Further, the time period for recording measurements from the stations was not consistent. In WY
256 2017, measurements began being reported on 10 November 2016 and were reported until 24
257 November 2017. However, in WY 2018, measurements weren't reported until 1 December 2017
258 and no station measurements were reported past 1 April 2017. The reporting period likely
259 covered all the snowfall events, but not all the precipitation events.

260 To address the rainfall measurement and reporting issues, we used GLDAS NOAH v2.1 (Rodell
261 et al., 2004) rainfall + snowfall from the nearest grid cell (1/4° spatial / 3 hr temporal resolution)
262 to fill in precipitation prior to the first measurements in each water year, and after 4-1 for both
263 water years. We did not account for rain from 10 November 2016 to 1 April 2017 and from 1
264 December 2017 to 1 April 2018; instead we relied on the modeled precipitation from
265 SNOWPACK using snow depth. The AKAH station observations show that rain during this time
266 period was rare.

267 5) A database problem prevented snow heights > 100 cm from being entered into the database
268 for a few days in 2017. This problem became apparent during February 2017, when the
269 Nuristan avalanches took place, as that is the first time that most stations recorded values >
270 100 cm. Values were shown as 100 cm on multiple days followed by values > 100 cm. To
271 address this issue, we flagged all the values equal to 100 cm prior to peak depth in 2017, then
272 marked those as null values. We then filled those null values using the cumulative sum of
273 new snow during that time.

274 5.5 Analysis of modeled snow profiles

275 For holistic measures of the snow profiles modeled in Alpine3D, we used two metrics from
276 Bellaire et al. (2018): 1) fraction of facets and 2) number of critical layers. Fraction of facets is
277 the height of all the layers containing faceted crystals, i.e. International Classification for



278 Seasonal Snow on the Ground primary codes FC, DH, and SH (Fierz et al., 2009), divided by the
279 height of the snowpack. The number of critical layers was computed using a threshold sum
280 approach (Schweizer and Jamieson, 2007) with modifications for simulated profiles (Monti et
281 al., 2014 Table 1). In each profile, 6 different variables (grain size, difference in grain size,
282 hardness, difference in hardness, grain type, and depth) in the top meter of height (from the
283 surface) were checked against threshold values. Layers exceeding 5 or more thresholds were
284 classified as critical.

285 The fraction of facets metric does not have a validation study, but faceted layers are a weak
286 crystal form and are responsible for 43% (Bair et al., 2012) to 67% (Schweizer and Jamieson,
287 2001) of investigated avalanches. Layers classified as critical using the threshold approach above
288 corresponded to failure layers about ½ of the time (Monti et al., 2014) in Compression Tests
289 (Jamieson, 1999; van Herwijnen and Jamieson, 2007), an in situ snowpack stability test.

290 5.6 Spatial scale for comparisons

291 Because ParBal is the only model run at 500 m spatial resolution and all the other models were
292 run at ~ 25 km, it is the only model appropriate for point comparisons, although point to area
293 problems are still an issue. To address the geolocational uncertainty for the gridded MODIS
294 products, which can be up to one ~500 m pixel (Tan et al., 2006; Xiaoxiong et al., 2005) and
295 spatial variability of the snow, we used a 9-pixel neighborhood centered on each AKAH station
296 and chose the best fit to the SNOWPACK modeled SWE. This approach has been used in
297 previous work (Bair et al., 2018b; Rittger et al., 2016).

298 For all of the other model comparisons, we resampled all of the model output to a UTM (Zone
299 43S) grid with 25 km pixels, close to the native resolution of the NOAH-MP and GLDAS2 grid
300 used (0.25°). The ParBal output had to be significantly upscaled from 500 m to 25 km using
301 Gaussian Pyramid reduction (Burt and Adelson, 1983) in steps with bilinear interpolation for the
302 final step.

303 6 RESULTS AND DISCUSSION

304 The relationships between the components are summarized in Figure 2. The results discussed
305 below are comparisons of: 1) SWE and 2) snow stratigraphy across a) all of the AKAH stations
306 (points) and b) the entire study region.

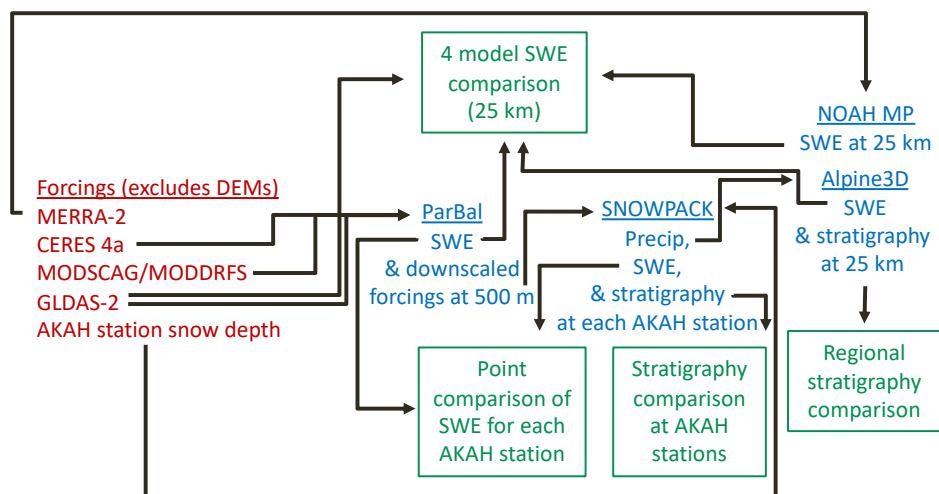


Figure 2 Summary of relationships between the various components. Forcings are shown in red, models and selected outputs are shown in blue, and the comparisons discussed below are shown in green. The black arrows show the direction of inputs.

307

308 6.1 Point comparisons between SNOWPACK and reconstructed SWE

309 A first step for any SWE reconstruction comparison is to determine when the ablation season
 310 starts. This varies for different years and at different sites (e.g. Margulis et al., 2016). Using the
 311 SNOWPACK modeled SWE, we can examine the peak SWE dates for both years for all of the
 312 AKAH stations (Figure 3ab). Peak SWE dates vary across the stations and years, but the median
 313 values are between years are a week apart, 19 February 2017 and 26 February 2018. Thus, we
 314 use those dates for our comparisons.

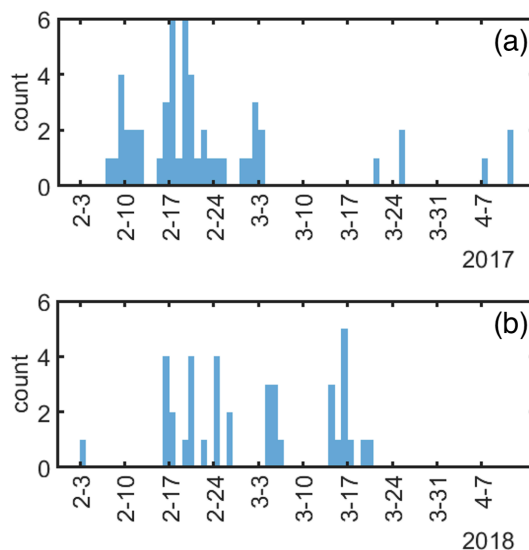


Figure 3 Peak SWE dates, modeled by SNOWPACK for 2017 (a) and 2018 (b) for each of the AKAH stations. The median peak SWE dates are 19 February 2017 and 26 February 2018. $N=52$ and 41 AKAH stations used for 2017 and 2018.

315

316 To create a holistic comparison for all the stations across the ablation period, mean SWE values
317 were computed and plotted for each day during the ablation season (Figure 4). For the
318 reconstructed SWE on 19 February 2017, the bias is -77 mm (-28%). For the reconstructed SWE
319 on 26 February 2018, the bias is -6 mm (-9%). Thus, together these biases average to -42 mm (-
320 19%). The increases in reconstructed SWE during the ablation season are caused due to
321 differences in how melt is summed for any given pixel. In ParBal, melt is only summed during
322 periods of contiguous snow cover. This means that if a pixel containing an AKAH station has no
323 snow on it at some point during the ablation season, but then snow is detected, it causes an
324 increase in the mean SWE. This is called an ephemeral snow event, i.e. snow that disappears and
325 reappears. For a more in depth examination of the error at individual stations, a box plot is
326 shown for the median peak SWE dates for both years (Figure 5). The median bias of the
327 reconstructed SWE is -11 mm (-14%).

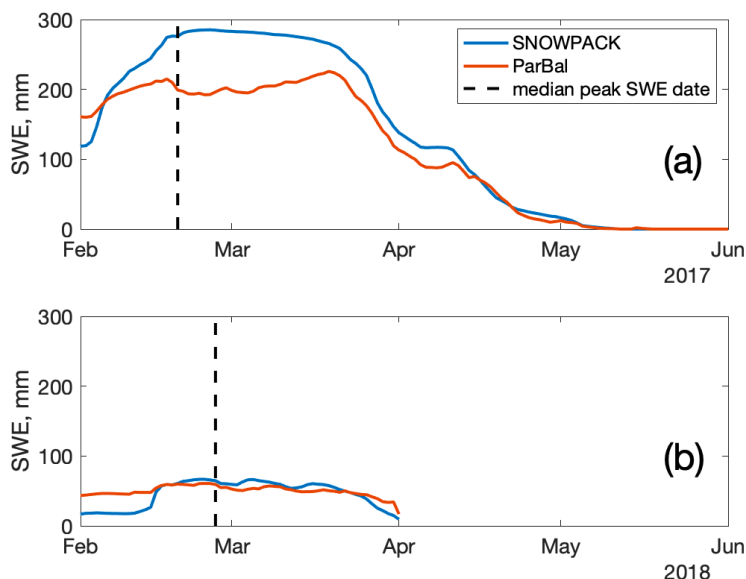


Figure 4 Mean SWE for 2017 (a) and 2018 (b) modeled at each of the AKAH stations using SNOWPACK compared to reconstructed SWE from ParBal using a best of 9 approach. Also plotted is the median peak SWE date. The modeled SWE values end abruptly on 1 April 2018 because the AKAH stations stopped reporting due to drought conditions. The number of stations used is the same as in Figure 3.

328
 329

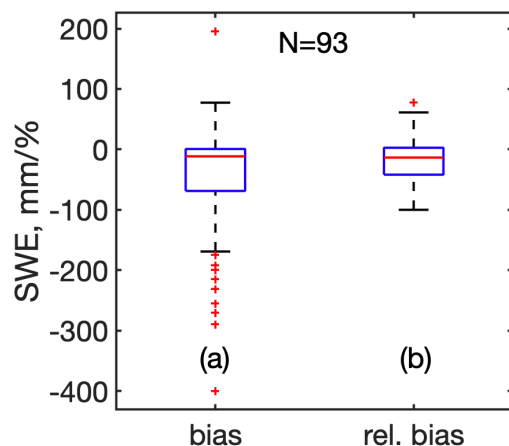


Figure 5 Bias (a) and relative bias (b) error for ParBal reconstructed SWE vs Alpine 3D modeled SWE at AKAH stations the median peak SWE date for both years, where bias here is ParBal SWE – Alpine 3D SWE.

330



331 6.2 Four model spatial comparisons

332 The AKAH stations are lower than the average elevation for the region. The average elevation of
333 the AKAH stations is 2619 m (1735 to 3410 m). But when the 500 m DEM is upscaled to 25 km,
334 the average elevation of the pixels containing the AKAH station is 3858 m with a range of 2517
335 to 4764 m. This has two important implications: 1) much of the higher elevation snowfall is
336 being extrapolated and 2) the higher elevation causes the peak SWE date to move forward in
337 time. The median peak SWE dates for the (N=169) 25 km pixels encompassing the study area
338 are 5 May 2017 and 3 May 2017. Thus, we use the median of the two to compare our
339 reconstructed SWE values (Figure 6ab and Figure 7a-d).

340 Striking is the range between models. NOAH-MP has the highest peaks (562 mm in 2017 and
341 331 mm in 2018), but is among the first to melt out. The reconstructed SWE from ParBal only
342 shows minor variation between the 2017 peak (240 mm) and the 2018 peak (206 mm). ParBal
343 and GLDAS-2 melt snow out latest in both years. The Alpine 3D model shows the second
344 highest peak SWE in 2017 (469 mm), but the lowest peak (165 mm) in 2018. The comparatively
345 higher values from NOAH-MP could result from relatively high precipitation estimates from its
346 MERRA2 precipitation forcings. Similarly, Viste and Sorteberg (2015) report that MERRA
347 (version 1) showed higher snowfall in the Indus Basin than any other reanalysis or observation-
348 based forcings dataset.

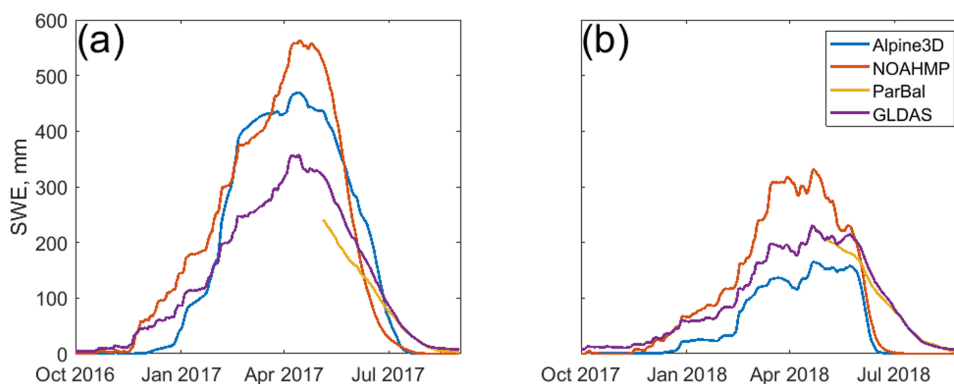


Figure 6 Time series of mean SWE for four snow models across the study area (13x13x25 km pixels) show in Figure 1 for 2017 (a) and 2018 (b). The reconstructed SWE from ParBal (yellow) goes back to 4 May, the median peak SWE date for both years, since reconstruction is only valid during the ablation season.

349

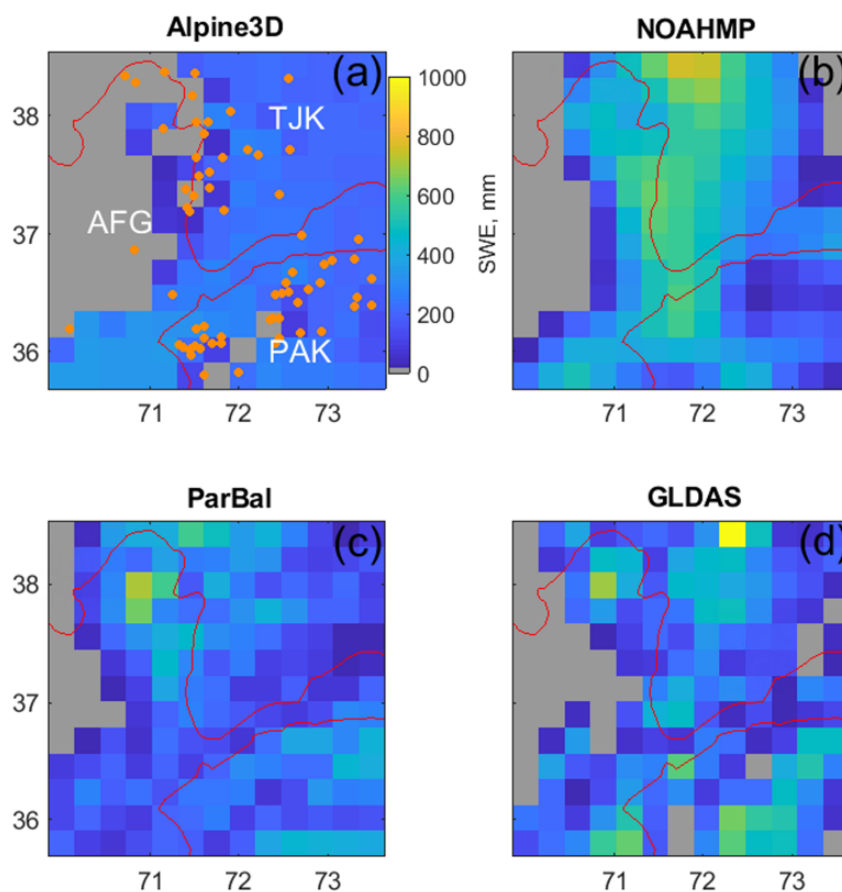


Figure 7 Four model (a-d) spatial comparison for the region on 4 May 2018. The white letters are the 3 letter ISO country codes (AFG–Afghanistan; TJK–Tajikistan; PAK–Pakistan). Also shown in (a) are the locations of the AKAH stations (orange points). This is a frame from a video sequence available as supplementary material.

350
351 Since Alpine3D is relying heavily on extrapolation of SWE, we suggest its mean SWE values
352 plotted in Figure 6 could have higher uncertainty than some of the other models. The ParBal
353 results are confounding given that the agreement between the modeled SWE from ParBal and
354 SNOWPACK at individual AKAH stations (Figure 4ab) is much better for both 2017 and 2018.
355 For insight into potential biases in the modeled spatial SWE from ParBal, we carefully studied
356 the snow-covered area (SCA, not just for 2017 & 2018, but since 2001), the potential melt (i.e.
357 the melt if a pixel were 100% snow covered), and the melt from glacierized areas (light blue in
358 Figure 1). We did not find any errors in the model, its parameters, or its forcings. Thus, it is
359 possible that the ParBal SWE is low-biased in 2017 for reasons that we could not discern, or that
360 the other models are high biased. Of note is that the 2017 & 2018 SCA (Figure 8 purple and



361 orange) is very similar for both years during the ablation period, especially at the end of the
362 ablation season.

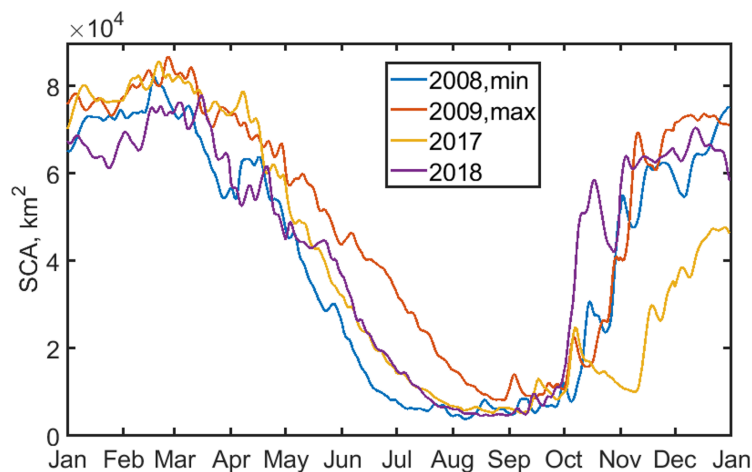


Figure 8 Time series of snow covered area from spatially and temporally interpolated MODSCAG (Rittger et al., in press), an input for ParBal, for four selected years across the region. Years 2008 and 2009 had the lowest and highest values on July 1 over the period of record from 2001 to 2018, while 2017 and 2018 comprise the AKAH station study period.

363
364 Since pixels do not contribute uniformly to melt, SCA alone cannot be used to predict SWE, but
365 in general years with less snow have lower SCA values towards the end of the ablation season.
366 Figure 8 shows that 2017 and 2018 were similar in terms of SCA from April through melt out.
367 Thus, the large difference between 2017 and 2018 for the AKAH station SWE, but small
368 differences in SCA and spatially-averaged reconstructed SWE, suggest that 2017 may have been
369 a larger snow year at the lower elevations where the AKAH stations are, but similar to 2018 at
370 the higher elevations.

371 6.3 Stratigraphy and stability

372 The simulated snow profiles from the AKAH stations (Figure 9ab) and the 25 km pixels
373 containing the AKAH stations (Figure 10ab) show very different snowpacks. Because of the
374 induced increase in elevation from scaling (e.g. from an average of 2619 m to 3858 m, Section
375 6.2), the 25 km pixels show a deeper, but more faceted snowpack with critical layers that persist
376 for a month or longer. In 2017, for the median AKAH station values, the snowpack reaches a
377 maximum of 76% facets on January 21 (Figure 9a). In 2018, the snowpack reaches a maximum
378 of 71% facets (Figure 9b). There were no critical layers simulated. In contrast, for the median
379 values in the 25 km pixels for both years, the height of snow (HS) is approximately $2 \times$ that for
380 the stations (Figure 10ab). The snowpack reaches a maximum of 94% facets in 2017, with one
381 critical layer persisting for 35 days (Figure 10a). The snowpack in 2018 reaches 95% facets with
382 1 or 2 critical layers persisting for 80 days (Figure 10b). During the Nuristan avalanches on 4
383 February to 7 February 2017 that killed over 100 people (United Nations, 2017), the AKAH
384 stations show the largest 3-day snowfall of the study period (Figure 9a) and the results for the 25



385 km pixels show that large snowfall occurring on top of the only critical layer of the season
386 (Figure 9b). That is a classic avalanche scenario, i.e. a large snowfall on a weak snowpack.

387 In lieu of any type of snow profile from this region, these profiles paint the best picture of the
388 snow conditions available. A relatively stable snowpack seems to be present in the valleys,
389 where the AKAH stations are located. But at the higher elevations, the simulated profiles show a
390 more dangerous snowpack. This is especially serious considering these villages are in the runout
391 zones of these unstable snowpacks. In some cases, several thousand meters of vertical relief
392 loom above the villages. For example, Yarkhun Lasht (36.795N 73.022E, el. 3249 m) in Pakistan
393 is flanked by 6500 m peaks on both side of its valley.

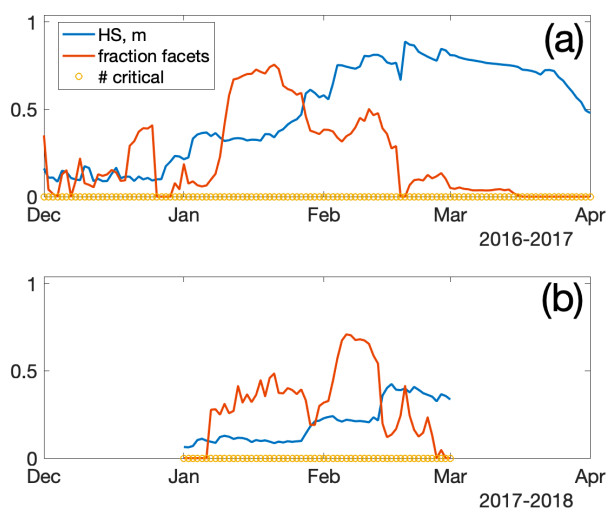


Figure 9 Stratigraphy summary of the AKAH stations for 2017 (a) and 2018 (b). Plotted are the median: height of snow (HS); fraction of the snowpack containing facets; and number of critical layers. The number of stations used to compute the medians varied due to snow coverage.

394



395

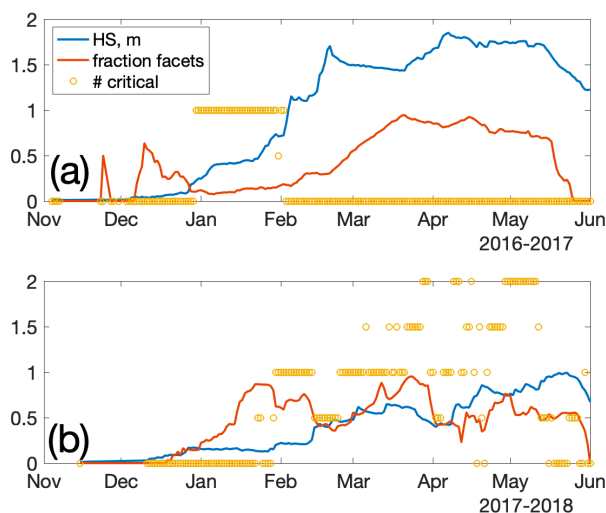


Figure 10 Stratigraphy summary of the (13x13) 25 km pixels containing AKAH stations for 2017 (a) and 2018 (b). Plotted are the median: height of snow (HS); fraction of the snowpack containing facets; and number of critical layers.

396

397 7 CONCLUSION

398 Thanks to a novel operational avalanche observation network, there are now daily snow
399 measurements at a number of operational weather stations in an austere region of High Mountain
400 Asia. In this study, two years of daily snow depth measurements from these stations were
401 combined with downscaled reanalysis and remotely-sensed measurements to force a point and
402 spatially distributed snow model. Compared to a previous effort (Bair et al., 2018b), this study
403 represents a substantial improvement in SWE modeling for the region, and a first attempt to
404 characterize region-wide snow stratigraphy. At the point scale, SWE estimates from a
405 reconstruction technique that does not use precipitation or in situ measurements compared
406 favorably. At the regional scale, four models showed a wide spread in both peak SWE and melt
407 timing. The simulated profiles showed very different snowpacks. At the point scale at lower
408 elevations in the valleys, profiles showed fewer facets and almost no critical layers, while at the
409 regional scale for higher elevations, the profiles showed heavily faceted snowpacks with critical
410 layers that persisted throughout the winter and spring.

411 8 CODE AND DATA AVAILABILITY

412 The code for ParBal is accessible at: <https://github.com/edwardbair/ParBal>

413 The code for MeteorIO, SNOWPACK, and Alpine3D are accessible at: <https://models.slf.ch/>

414 The code for NOAH-MP is accessible at: [https://ral.ucar.edu/solutions/products/noah-](https://ral.ucar.edu/solutions/products/noah-multiparameterization-land-surface-model-noah-mp-lsm)
415 [multiparameterization-land-surface-model-noah-mp-lsm](https://ral.ucar.edu/solutions/products/noah-multiparameterization-land-surface-model-noah-mp-lsm)



416 The GLDAS-2 and MERRA-2 forcings are accessible at: <https://disc.gsfc.nasa.gov/>
417 The reconstructed SWE and melt cubes are accessible at:
418 <ftp://ftp.snow.ucsb.edu/pub/org/snow/products/reconstruction/h23v05/500m/>
419 Unfortunately, the AKAH measurements are not publicly available due to security concerns.
420 Requests for the dataset should be made through The Aga Khan Agency for Habitat
421 (<https://www.akdn.org>).



422 **APPENDIX A Detailed model forcings and parameters**

423 *PARBAL*

424 ParBal was configured and forced as described in Bair et al. (2018b); Bair et al. (2016). The
 425 model time step was 1 hr. The DEM used was the ASTER GDEM version 2 at 1 arc sec (NASA
 426 JPL, 2011), while the canopy type and fraction were taken from the Global Land Survey at 30 m
 427 (USGS, 2009). The shortwave and longwave forcings were downscaled from the CERES SYN
 428 edition 4a 1°/1 hr product (Rutan et al., 2015), while the air temperature, specific humidity, air
 429 pressure, and wind speeds were downscaled from the GLDAS NOAH version 2.1 0.25°/3 hr
 430 product (Cosgrove et al., 2003). Time-space smoothed (Dozier et al., 2008; Rittger et al., in
 431 press) fSCA and grain size from MODSCAG (Painter et al., 2009) was combined with the
 432 visible albedo degradation from dust in MODDRFS (Painter et al., 2012) to produce snow hourly
 433 snow albedo.

434 *NOAH-MP*

435 NOAH-MP v3.6 was run in retrospective mode within the NASA Land Information System
 436 (LIS) framework. A state vector ensemble (total 30 replicates) was generated by perturbing the
 437 forcings to account for the state uncertainty during forward propagation of the model. MERRA-2
 438 (Gelaro et al., 2017) forcings were utilized with bilinear spatial and linear temporal interpolation.
 439 The model was run on an equidistant cylindrical grid with 0.25° spatial resolution and a 15 min
 440 model timestep. The spin-up time extended from May 2002 to May 2016 while the study period
 441 was from June 2016 to October 2018. The number of maximum layers in the snowpack was 3.
 442 Table A1 provides details of the NOAH-MP scheme options selected. Further details regarding
 443 each scheme and relevant references can be found at:
 444 [https://ral.ucar.edu/solutions/products/noah-multiparameterization-land-surface-model-noah-mp-](https://ral.ucar.edu/solutions/products/noah-multiparameterization-land-surface-model-noah-mp-lsm)
 445 [lsm.](https://ral.ucar.edu/solutions/products/noah-multiparameterization-land-surface-model-noah-mp-lsm)

Physical process/ parameter	Scheme used
Elevation data	SRTM Native
Landcover data	MODIS Native (IGBPNCCEP)
Slope, Albedo and Greenness data	NCEP Native
Bottom temperature (lapse-rate correction)	ISLSCP1
Vegetation	dynamic
Canopy stomatal resistance	Ball-Berry
Runoff and groundwater	SIMGM
Surface layer drag coefficient	M-O (General Monin-Obukhov similarity theory)
Supercooled liquid water and frozen soil permeability	NY06
Radiation transfer	gap=F(3D;cosz)



Snow surface albedo	BATS (Biosphere-Atmosphere Transfer Scheme)
Rainfall and snowfall	Jordan91
Snow and soil temperature time	semi-implicit
Lower boundary of soil temperature	Noah

446 *Table A1 Noah-MP v3.6 physical parametrization scheme options utilized in this study.*

447 **SNOWPACK**

448 SNOWPACK v3.50 was run in research mode at a 15 min timestep with hourly outputs for each
 449 of the AKAH stations. Hourly forcings were computed by combining temporally interpolated
 450 snow depth from the AKAH manual measurements with: air temperature, incoming shortwave,
 451 reflected shortwave, incoming longwave, wind speed, and relative humidity from the downscaled
 452 ParBal outputs, as described in Section 5.2. SNOWPACK was only run for periods when
 453 measurements from the AKAH stations were available, Nov/Dec to April/May, depending on the
 454 year.

455 Plots were assumed to be level, so forcings without terrain correction were applied except for
 456 shading when the sun was below the local horizon, e.g. a mountain blocking the sun (Dozier and
 457 Frew, 1990). The wind direction, which is not available in GLDAS-2, was fixed at the mean
 458 value from the daily AKAH instantaneous values. The ground temperature was set as the
 459 minimum of the air temperature or -1.5°C when snow cover was present.

460 Aside from setting required parameters and values for inputs and outputs, changes to default
 461 parameters that affected model output are provided in Table A2:

Parameters	Value	Description
TS_DAYS_BETWEEN	0.014666 days	Output hourly values
PRECIP_RATES	FALSE	Output is provided a summed precipitation over the output timestep (1 hr)
SW_MODE	BOTH	Both incoming and reflected (incoming x albedo) are provided
HEIGHT_OF_METEO_VALUES	2 m	Height of meteorological measurements
HEIGHT_OF_WIND_VALUE	2 m	Height of wind measurements
ENFORCE_MEASURED_SNOW_HEIGHTS	TRUE	Precipitation is calculated using HS
ATMOSPHERIC_STABILITY	NEUTRAL	Neutral conditions are often present in moderate to high wind speeds for mountain terrain (Lehning et al., 2002a; Mitterer and Schweizer, 2013)
MEAS_INCOMING_LONGWAVE	TRUE	Default is to estimate



	emissivity of the air and incoming longwave from other measured parameters (FALSE). Here we provide longwave forcings (TRUE).
--	---

462 *Table A2 Model parameters for SNOWPACK*

463 *ALPINE3D*

464 Alpine3D version 3.10 was run using with the outputs produced by SNOWPACK as forcings for
 465 each of the AKAH stations at 25 km resolution. The DEM and land cover (incorrectly labeled
 466 land use in the Alpine3D documentation) data were upscaled from the ParBal data. Alpine3D
 467 was run at an hourly timestep using hourly forcings, with daily outputs using the “enable-eb”
 468 switch. Other switches were set to off, the defaults. The “enable-eb” switch computes the terrain
 469 radiation with shading and terrain reflections (see Alpine 3D documentation at
 470 <https://models.slf.ch> for a description).

471 To extend the length of the model runs, for each AKAH stations, GLDAS-2 precipitation was
 472 appended to periods prior to the first AKAH observation for the year and after the last, as
 473 described in Section 5.4.

474 The forcings were hourly: incoming shortwave, incoming longwave, air temperature, relative
 475 humidity, wind speed, wind direction, reflected shortwave, accumulated precipitation, and
 476 ground temperature.

477 Critical to Alpine3D are the interpolation methods from MeteIO to spatially distribute
 478 precipitation and other forcings. We found the modeled SWE to be highly dependent on the
 479 spatial interpolation of precipitation. Our initial approach was to explore local (i.e. with a given
 480 radius from a station) and regional (i.e. all AKAH stations) lapse rates in the measured snow
 481 depth and modeled precipitation from SNOWPACK. We found almost no correlation in many of
 482 the measurements, not surprising given the complexity of the terrain and likely existence of
 483 microclimates with substantial influence on precipitation. Without having a good validation
 484 source for spatial precipitation (as is the case for all of High Mountain Asia), we selected an
 485 interpolation method that yielded relatively smooth results, but showed increases in precipitation
 486 with elevation.

487 Ultimately, we decided to use an inverse distance weighting scheme with elevation detrending
 488 (IDW_LAPSE) and a multilinear option. For this method, the input data are detrended, then the
 489 residuals are spatially interpolated according to an inverse distance weighting scheme. The
 490 detrending uses a multiple linear regression with northing, easting, and altitude. The linear
 491 regression has an iterative method for removing outliers. Finally, values at each cell are
 492 retrended using the multiple linear regression and added to the interpolated residuals.

493 A summary of the interpolation methods, all of which are defined in the MeteIO documentation
 494 (Bavay and Egger, 2014), is given in Table A3.

Forcing	Spatial interpolation method	Description and notes
Air temperature	IDW_LAPSE	Inverse distance weighting with elevation detrending.



Accumulated precipitation	IDW_LAPSE with multilinear option set to TRUE	See notes above
Relative Humidity	LISTON_RH	See Liston and Elder (2006)
Precipitation phase	PPHASE	Simple splitting at 274.35K
Wind speed	IDW_LAPSE	See above
Incoming longwave radiation	AVG_LAPSE	Average filling with elevation lapse rate
Wind direction	CST	Constant, fixed at average value from AKAH station instantaneous measurements
Pressure	STD_PRESS	Standard atmospheric pressure with elevation

495 *Table A3 Spatial interpolation methods for Alpine3D*

496 The same parameters as in Table A2 for SNOWPACK were used in Alpine3D with changes
 497 shown in Table A4. Other parameters were defaults.

Parameters	Value	Description
CALCULATION_STEP_LENGTH	60 min	1 hr model timestep
ENFORCE_MEASURED_SNOW_HEIGHTS	FALSE	Use accumulated precipitation estimate from SNOWPACK

498 *Table A4 Model parameter changes for Alpine3D from Table A2*

499 AUTHOR CONTRIBUTION

500 DC provided the AKAH dataset. JA ran the NOAH MP simulations. KR prepared the snow
 501 surface properties dataset. EB processed the data and prepared the manuscript.

502 COMPETING INTERESTS

503 The authors declare that they have no conflicts of interest.

504 ACKNOWLEDGMENTS

505 We are grateful to the Aga Khan Agency for Habitat for supplying the first snow measurements
 506 in Afghanistan's watersheds since the 1980s. This work was supported by NASA Awards
 507 80NSSC18K0427, 80NSSC18K1489, NASA 2015 HiMAT, and NNX17AC15G.

508

509 REFERENCES

510 Adam, J. C., Clark, E. A., Lettenmaier, D. P., and Wood, E. F.: Correction of global precipitation
 511 products for orographic effects, *Journal of Climate*, 19, 15-38, doi 10.1175/JCLI3604.1, 2006.



- 512 Armstrong, R. L., Rittger, K., Brodzik, M. J., and others: Runoff from glacier ice and seasonal snow in
513 High Asia: separating melt water sources in river flow, *Regional Environmental Change*, 1-13, doi
514 <https://doi.org/10.1007/s10113-018-1429-0>, 2018.
- 515 Bair, E. H., Davis, R. E., and Dozier, J.: Hourly mass and snow energy balance measurements from
516 Mammoth Mountain, CA USA, 2011–2017, *Earth Syst. Sci. Data*, 10, 549-563, doi 10.5194/essd-10-549-
517 2018, 2018a.
- 518 Bair, E. H., Simenhois, R., Birkeland, K., and Dozier, J.: A field study on failure of storm snow slab
519 avalanches, *Cold Regions Science and Technology*, 79-80, 20-28, doi 10.1016/j.coldregions.2012.02.007,
520 2012.
- 521 Bair, E. H., Abreu Calfa, A., Rittger, K., and Dozier, J.: Using machine learning for real-time estimates of
522 snow water equivalent in the watersheds of Afghanistan, *The Cryosphere*, 12, 1579-1594, doi 10.5194/tc-
523 12-1579-2018, 2018b.
- 524 Bair, E. H., Rittger, K., Davis, R. E., Painter, T. H., and Dozier, J.: Validating reconstruction of snow
525 water equivalent in California's Sierra Nevada using measurements from the NASA Airborne Snow
526 Observatory, *Water Resources Research*, 52, 8437-8460, doi 10.1002/2016WR018704, 2016.
- 527 Bartelt, P., and Lehning, M.: A physical SNOWPACK model for the Swiss avalanche warning: Part I:
528 numerical model, *Cold Regions Science and Technology*, 35, 123-145, doi 10.1016/s0165-
529 232x(02)00074-5, 2002.
- 530 Bavay, M., and Egger, T.: MeteoIO 2.4.2: a preprocessing library for meteorological data, *Geosci. Model
531 Dev.*, 7, 3135-3151, doi 10.5194/gmd-7-3135-2014, 2014.
- 532 Bellaire, S., Jamieson, J. B., and Fierz, C.: Forcing the snow-cover model SNOWPACK with forecasted
533 weather data, *The Cryosphere*, 5, 1115-1125, doi 10.5194/tc-5-1115-2011, 2011.
- 534 Bellaire, S., van Herwijnen, A., Bavay, M., and Schweizer, J.: Distributed modeling of snow cover
535 instability at regional scale, *Proceedings of the 2018 International Snow Science Workshop, Innsbruck,
536 Austria*, 2018, 871-875,
- 537 Bookhagen, B., and Burbank, D. W.: Toward a complete Himalayan hydrological budget: Spatiotemporal
538 distribution of snowmelt and rainfall and their impact on river discharge, *Journal of Geophysical
539 Research: Earth Surface*, 115, doi 10.1029/2009jf001426, 2010.
- 540 Burt, P., and Adelson, E.: The Laplacian pyramid as a compact image code, *IEEE Transactions on
541 Communications*, 31, 532-540, doi 10.1109/TCOM.1983.1095851, 1983.
- 542 Chabot, D., and Kaba, A.: Avalanche forecasting in the central Asian countries of Afghanistan, Pakistan
543 and Tajikistan, *Proc. 2016 Intl. Snow Sci. Wksp., Breckenridge, CO*, 2016,
544 <http://arc.lib.montana.edu/snow-science/item/2310>.
- 545 Chen, F., Barlage, M., Tewari, M., Rasmussen, R., Jin, J., Lettenmaier, D., Livneh, B., Lin, C., Miguez-
546 Macho, G., Niu, G.-Y., Wen, L., and Yang, Z.-L.: Modeling seasonal snowpack evolution in the complex
547 terrain and forested Colorado Headwaters region: A model intercomparison study, *Journal of Geophysical
548 Research: Atmospheres*, 119, 13,795-713,819, doi 10.1002/2014jd022167, 2014.



- 549 Cornwell, E., Molotch, N. P., and McPhee, J.: Spatio-temporal variability of snow water equivalent in the
550 extra-tropical Andes Cordillera from distributed energy balance modeling and remotely sensed snow
551 cover, *Hydrol. Earth Syst. Sci.*, 20, 411-430, doi 10.5194/hess-20-411-2016, 2016.
- 552 Cosgrove, B. A., Lohmann, D., Mitchell, K. E., Houser, P. R., Wood, E. F., Schaake, J. C., Robock, A.,
553 Marshall, C., Sheffield, J., Duan, Q., Luo, L., Higgins, R. W., Pinker, R. T., Tarpley, J. D., and Meng, J.:
554 Real-time and retrospective forcing in the North American Land Data Assimilation System (NLDAS)
555 project, *Journal of Geophysical Research: Atmospheres*, 108, 8842, doi 10.1029/2002JD003118, 2003.
- 556 Dahri, Z. H., Ludwig, F., Moors, E., Ahmad, B., Khan, A., and Kabat, P.: An appraisal of precipitation
557 distribution in the high-altitude catchments of the Indus basin, *Science of The Total Environment*, 548-
558 549, 289-306, doi <https://doi.org/10.1016/j.scitotenv.2016.01.001>, 2016.
- 559 Dahri, Z. H., Moors, E., Ludwig, F., Ahmad, S., Khan, A., Ali, I., and Kabat, P.: Adjustment of
560 measurement errors to reconcile precipitation distribution in the high-altitude Indus basin, *Int. J.*
561 *Climatol.*, 38, 3842-3860, doi 10.1002/joc.5539, 2018.
- 562 Dozier, J., and Frew, J.: Rapid calculation of terrain parameters for radiation modeling from digital
563 elevation data, *IEEE Transactions on Geoscience and Remote Sensing*, 28, 963-969, doi
564 10.1109/36.58986, 1990.
- 565 Dozier, J., Painter, T. H., Rittger, K., and Frew, J. E.: Time-space continuity of daily maps of fractional
566 snow cover and albedo from MODIS, *Advances in Water Resources*, 31, 1515-1526, doi
567 10.1016/j.advwatres.2008.08.011, 2008.
- 568 Ek, M. B., Mitchell, K. E., Lin, Y., Rogers, E., Grunmann, P., Koren, V., Gayno, G., and Tarpley, J. D.:
569 Implementation of Noah land surface model advances in the National Centers for Environmental
570 Prediction operational mesoscale Eta model, *Journal of Geophysical Research: Atmospheres*, 108, doi
571 10.1029/2002jd003296, 2003.
- 572 Fierz, C., Armstrong, R. L., Durand, Y., Etchevers, P., Greene, E., McClung, D. M., Nishimura, K.,
573 Satyawali, P. K., and Sokratov, S.: The International Classification for Seasonal Snow on the Ground,
574 IHP-VII Technical Documents in Hydrology N°83, 90, 2009.
- 575 Gelaro, R., McCarty, W., Suárez, M. J., Todling, R., Molod, A., Takacs, L., Randles, C. A., Darmenov,
576 A., Bosilovich, M. G., Reichle, R., Wargan, K., Coy, L., Cullather, R., Draper, C., Akella, S., Buchard,
577 V., Conaty, A., Silva, A. M. d., Gu, W., Kim, G.-K., Koster, R., Lucchesi, R., Merkova, D., Nielsen, J. E.,
578 Partyka, G., Pawson, S., Putman, W., Rienecker, M., Schubert, S. D., Sienkiewicz, M., and Zhao, B.: The
579 Modern-Era Retrospective Analysis for Research and Applications, Version 2 (MERRA-2), *Journal of*
580 *Climate*, 30, 5419-5454, doi 10.1175/jcli-d-16-0758.1, 2017.
- 581 Goodison, B., Louie, P. Y. T., and Yang, D.: WMO Solid precipitation measurement intercomparison,
582 World Meteorological Organization, 1998.
- 583 Harris, I., Jones, P. D., Osborn, T. J., and Lister, D. H.: Updated high-resolution grids of monthly climatic
584 observations – the CRU TS3.10 Dataset, *Int. J. Climatol.*, 34, 623-642, doi 10.1002/joc.3711, 2014.
- 585 Hirashima, H., Yamaguchi, S., Sato, A., and Lehning, M.: Numerical modeling of liquid water movement
586 through layered snow based on new measurements of the water retention curve, *Cold Regions Science*
587 *and Technology*, 64, 94-103, doi <https://doi.org/10.1016/j.coldregions.2010.09.003>, 2010.



- 588 Huffman, G. J., Bolvin, D. T., Nelkin, E. J., Wolff, D. B., Adler, R. F., Gu, G., Hong, Y., Bowman, K. P.,
589 and Stocker, E. F.: The TRMM Multisatellite Precipitation Analysis (TMPA): Quasi-Global, Multiyear,
590 Combined-Sensor Precipitation Estimates at Fine Scales, *J. Hydrometeorol.*, 8, 38-55, doi
591 10.1175/jhm560.1, 2007.
- 592 Immerzeel, W. W., Wanders, N., Lutz, A. F., Shea, J. M., and Bierkens, M. F. P.: Reconciling high-
593 altitude precipitation in the upper Indus basin with glacier mass balances and runoff, *Hydrol. Earth Syst.*
594 *Sci.*, 19, 4673-4687, doi 10.5194/hess-19-4673-2015, 2015.
- 595 Jamieson, J. B.: The compression test – after 25 years, *The Avalanche Review*, 18, 10-12, 1999.
- 596 Jepsen, S. M., Molotch, N. P., Williams, M. W., Rittger, K. E., and Sickman, J. O.: Interannual variability
597 of snowmelt in the Sierra Nevada and Rocky Mountains, United States: Examples from two alpine
598 watersheds, *Water Resources Research*, 48, W02529, doi 10.1029/2011WR011006, 2012.
- 599 Kochendorfer, J., Rasmussen, R., Wolff, M., Baker, B., Hall, M. E., Meyers, T., Landolt, S., Jachcik, A.,
600 Isaksen, K., Brækkan, R., and Leeper, R.: The quantification and correction of wind-induced precipitation
601 measurement errors, *Hydrol. Earth Syst. Sci.*, 21, 1973-1989, doi 10.5194/hess-21-1973-2017, 2017.
- 602 Lehning, M., Bartelt, P., Brown, B., and et. al: SNOWPACK model calculations for avalanche warning
603 based upon a new network of weather and snow stations, *Cold Reg. Sci. Technol.*, 30, 145-157, 1999.
- 604 Lehning, M., Bartelt, P., Brown, B., and Fierz, C.: A physical SNOWPACK model for the Swiss
605 avalanche warning: Part III: meteorological forcing, thin layer formation and evaluation, *Cold Regions*
606 *Science and Technology*, 35, 169-184, doi 10.1016/S0165-232X(02)00072-1, 2002a.
- 607 Lehning, M., Bartelt, P., Brown, B., Fierz, C., and Satyawali, P.: A physical SNOWPACK model for the
608 Swiss avalanche warning, Part II: Snow microstructure, *Cold Regions Science and Technology*, 35, 147-
609 167, doi: 110.1016/S0165-1232X(1002)00073-00073, 2002b.
- 610 Lehning, M., Völsch, I., Gustafsson, D., Nguyen, T. A., Stähli, M., and Zappa, M.: ALPINE3D: a
611 detailed model of mountain surface processes and its application to snow hydrology, *Hydrological*
612 *Processes*, 20, 2111-2128, doi 10.1002/hyp.6204, 2006.
- 613 Liston, G. E., and Elder, K.: A meteorological distribution system for high-resolution terrestrial modeling
614 (MicroMet), *J. Hydrometeorol.*, 7, 217–234, doi 10.1175/JHM486.1, 2006.
- 615 Lutz, A. F., Immerzeel, W. W., Shrestha, A. B., and Bierkens, M. F. P.: Consistent increase in High
616 Asia’s runoff due to increasing glacier melt and precipitation, *Nature Climate Change*, 4, 587, doi
617 10.1038/nclimate2237, 2014.
- 618 Margulis, S. A., Cortés, G., Giroto, M., and Durand, M.: A Landsat-Era Sierra Nevada Snow Reanalysis
619 (1985–2015), *J. Hydrometeorol.*, 17, 1203-1221, doi 10.1175/jhm-d-15-0177.1, 2016.
- 620 Martinec, J., and Rango, A.: Areal distribution of snow water equivalent evaluated by snow cover
621 monitoring, *Water Resources Research*, 17, 1480-1488, doi 10.1029/WR017i005p01480, 1981.
- 622 Milly, P. C. D., and Dunne, K. A.: Macroscale water fluxes 1. Quantifying errors in the estimation of
623 basin mean precipitation, *Water Resources Research*, 38, 23-21-23-14, doi 10.1029/2001WR000759,
624 2002.



- 625 Mitterer, C., and Schweizer, J.: Analysis of the snow-atmosphere energy balance during wet-snow
626 instabilities and implications for avalanche prediction, *The Cryosphere*, 7, 205-216, doi 10.5194/tc-7-205-
627 2013, 2013.
- 628 Molotch, N. P.: Reconstructing snow water equivalent in the Rio Grande headwaters using remotely
629 sensed snow cover data and a spatially distributed snowmelt model, *Hydrological Processes*, 23, 1076-
630 1089, doi 10.1002/hyp.7206, 2009.
- 631 Monti, F., Schweizer, J., and Fierz, C.: Hardness estimation and weak layer detection in simulated snow
632 stratigraphy, *Cold Regions Science and Technology*, 103, 82-90, doi
633 <https://doi.org/10.1016/j.coldregions.2014.03.009>, 2014.
- 634 Nishimura, K., Baba, E., Hirashima, H., and Lehning, M.: Application of the snow cover model
635 SNOWPACK to snow avalanche warning in Niseko, Japan, *Cold Regions Science and Technology*, 43,
636 62-70, doi <https://doi.org/10.1016/j.coldregions.2005.05.007>, 2005.
- 637 Niu, G.-Y., and Yang, Z.-L.: Effects of vegetation canopy processes on snow surface energy and mass
638 balances, *Journal of Geophysical Research: Atmospheres*, 109, doi 10.1029/2004jd004884, 2004.
- 639 Niu, G.-Y., Yang, Z.-L., Mitchell, K. E., Chen, F., Ek, M. B., Barlage, M., Kumar, A., Manning, K.,
640 Niyogi, D., Rosero, E., Tewari, M., and Xia, Y.: The community Noah land surface model with
641 multiparameterization options (Noah-MP): 1. Model description and evaluation with local-scale
642 measurements, *Journal of Geophysical Research: Atmospheres*, 116, doi 10.1029/2010jd015139, 2011.
- 643 Painter, T. H., Bryant, A. C., and Skiles, S. M.: Radiative forcing by light absorbing impurities in snow
644 from MODIS surface reflectance data, *Geophysical Research Letters*, 39, L17502, doi
645 10.1029/2012GL052457, 2012.
- 646 Painter, T. H., Rittger, K., McKenzie, C., Slaughter, P., Davis, R. E., and Dozier, J.: Retrieval of subpixel
647 snow-covered area, grain size, and albedo from MODIS, *Remote Sensing of Environment*, 113, 868-879,
648 doi 10.1016/j.rse.2009.01.001, 2009.
- 649 Raup, B., Racoviteanu, A., Khalsa, S. J. S., Helm, C., Armstrong, R., and Arnaud, Y.: The GLIMS
650 geospatial glacier database: A new tool for studying glacier change, *Global and Planetary Change*, 56,
651 101-110, doi <https://doi.org/10.1016/j.gloplacha.2006.07.018>, 2007.
- 652 Rienecker, M. M., Suarez, M. J., Gelaro, R., Todling, R., Julio Bacmeister, Liu, E., Bosilovich, M. G.,
653 Schubert, S. D., Takacs, L., Kim, G.-K., Bloom, S., Chen, J., Collins, D., Conaty, A., Silva, A. d., Gu, W.,
654 Joiner, J., Koster, R. D., Lucchesi, R., Molod, A., Owens, T., Pawson, S., Pegion, P., Redder, C. R.,
655 Reichle, R., Robertson, F. R., Ruddick, A. G., Sienkiewicz, M., and Woollen, J.: MERRA: NASA's
656 Modern-Era Retrospective Analysis for Research and Applications, *Journal of Climate*, 24, 3624-3648,
657 doi 10.1175/jcli-d-11-00015.1, 2011.
- 658 Rittger, K., Bair, E. H., Kahl, A., and Dozier, J.: Spatial estimates of snow water equivalent from
659 reconstruction, *Advances in Water Resources*, 94, 345-363, doi 10.1016/j.advwatres.2016.05.015, 2016.
- 660 Rittger, K., Raleigh, M. S., Dozier, J., Hill, A. F., Lutz, J. A., and Painter, T. H.: Canopy Adjustment and
661 Improved Cloud Detection for Remotely Sensed Snow Cover Mapping, *Water Resources Research*, in
662 press.



- 663 Rodell, M., Houser, P. R., Jambor, U., Gottschalck, J., Mitchell, K., Meng, C. J., Arsenault, K., Cosgrove,
664 B., Radakovich, J., Bosilovich, M., Entin, J. K., Walker, J. P., Lohmann, D., and Toll, D.: The Global
665 Land Data Assimilation System, *Bulletin of the American Meteorological Society*, 85, 381-394, doi
666 10.1175/BAMS-85-3-381, 2004.
- 667 Rutan, D. A., Kato, S., Doelling, D. R., Rose, F. G., Nguyen, L. T., Caldwell, T. E., and Loeb, N. G.:
668 CERES synoptic product: Methodology and validation of surface radiant flux, *J. Atmos. Ocean. Technol.*,
669 32, 1121-1143, doi 10.1175/JTECH-D-14-00165.1, 2015.
- 670 Schweizer, J., and Jamieson, B.: Snow cover properties for skier triggering of avalanches, *Cold Regions
671 Science and Technology*, 33, 207-221, doi 10.1016/s0165-232x(01)00039-8, 2001.
- 672 Schweizer, J., and Jamieson, B.: A threshold sum approach to stability evaluation of manual snow
673 profiles, *Cold Regions Science and Technology*, 47, 50-59, doi 10.1016/j.coldregions.2006.08.011, 2007.
- 674 Shakoor, A., and Ejaz, N.: Flow Analysis at the Snow Covered High Altitude Catchment via Distributed
675 Energy Balance Modeling, *Scientific Reports*, 9, 4783, doi 10.1038/s41598-019-39446-1, 2019.
- 676 Smith, T., and Bookhagen, B.: Changes in seasonal snow water equivalent distribution in High Mountain
677 Asia (1987 to 2009), *Science Advances*, 4, e1701550, doi 10.1126/sciadv.1701550, 2018.
- 678 Sturm, M., Holmgren, J., and Liston, G. E.: A seasonal snow cover classification system for local to
679 global applications, *Journal of Climate*, 8, 1261-1283, doi 10.1175/1520-
680 0442(1995)008<1261:ASSCCS>2.0.CO;2, 1995.
- 681 Sturm, M., Taras, B., Liston, G. E., Derksen, C., Jonas, T., and Lea, J.: Estimating snow water equivalent
682 using snow depth data and climate classes, *J. Hydrometeorol.*, 11, 1380-1394, doi
683 10.1175/2010jhm1202.1, 2010.
- 684 Tan, B., Woodcock, C. E., Hu, J., Zhang, P., Ozdogan, M., Huang, D., Yang, W., Knyazikhin, Y., and
685 Myneni, R. B.: The impact of gridding artifacts on the local spatial properties of MODIS data:
686 Implications for validation, compositing, and band-to-band registration across resolutions, *Remote
687 Sensing of Environment*, 105, 98-114, doi 10.1016/j.rse.2006.06.008, 2006.
- 688 United Nations: Afghanistan: Nuristan avalanche, update to flash report (as of 8 February 2017), Office
689 for the Coordination of Humanitarian Affairs (OCHA), 2017.
- 690 USAID: Afghanistan Food Security Update, FEWS Net, Washington, DC, 4, 2008.
- 691 USGS: Global Land Survey: <http://glcfapp.glcf.umd.edu/data/gls/>, access: 1 September 2017, 2009.
- 692 van Herwijnen, A., and Jamieson, B.: Fracture character in compression tests, *Cold Regions Science and
693 Technology*, 47, 60-68, doi 10.1016/j.coldregions.2006.08.016, 2007.
- 694 Viste, E., and Sorteberg, A.: Snowfall in the Himalayas: an uncertain future from a little-known past, *The
695 Cryosphere*, 9, 1147-1167, doi 10.5194/tc-9-1147-2015, 2015.
- 696 Xia, Y., Mitchell, K., Ek, M., Sheffield, J., Cosgrove, B., Wood, E., Luo, L., Alonge, C., Wei, H., Meng,
697 J., Livneh, B., Lettenmaier, D., Koren, V., Duan, Q., Mo, K., Fan, Y., and Mocko, D.: Continental-scale
698 water and energy flux analysis and validation for the North American Land Data Assimilation System



- 699 project phase 2 (NLDAS-2): 1. Intercomparison and application of model products, Journal of
700 Geophysical Research: Atmospheres, 117, D03109, doi 10.1029/2011JD016048, 2012.
- 701 Xiaoxiong, X., Nianzeng, C., and Barnes, W.: Terra MODIS on-orbit spatial characterization and
702 performance, IEEE Transactions on Geoscience and Remote Sensing, 43, 355-365, doi
703 10.1109/TGRS.2004.840643, 2005.
- 704 Yang, Z.-L., and Niu, G.-Y.: The Versatile Integrator of Surface and Atmosphere processes: Part 1.
705 Model description, Global and Planetary Change, 38, 175-189, doi [https://doi.org/10.1016/S0921-](https://doi.org/10.1016/S0921-8181(03)00028-6)
706 [8181\(03\)00028-6](https://doi.org/10.1016/S0921-8181(03)00028-6), 2003.
- 707 Yatagai, A., Kamiguchi, K., Arakawa, O., Hamada, A., Yasutomi, N., and Kitoh, A.: APHRODITE:
708 Constructing a Long-Term Daily Gridded Precipitation Dataset for Asia Based on a Dense Network of
709 Rain Gauges, Bulletin of the American Meteorological Society, 93, 1401-1415, doi 10.1175/bams-d-11-
710 00122.1, 2012.
711